Eidgenössische Technische Hochschule Zürich
Swiss Federal Institute of Technology Zurich

# Bachelor Thesis

## Correlation Function Measurements for Circuit Quantum Electrodynamics

Laboratory for Solid State Physics
ETH Zürich, Switzerland

| | |
|---|---|
| Presented by: | Gebhard Littich |
| Carried out at: | Quantum Device Lab |
| Supervisors: | Dr. Peter Leek |
| | Prof. Dr. Andreas Wallraff |

Zürich, July 2009

# Abstract

Recent work [1], [2], [3] has been done on establishing and characterizing microwave beam splitters for applications in the field of circuit quantum electrodynamics. It was shown that an equivalent to optical devices can be fabricated based on superconducting circuitry. As tests have shown that produced beam splitters work within an appropriate frequency range and split incident signals with almost 50:50 ratio, one can head towards performing quantum mechanical experiments incorporating single-photon sources and entanglement of certain input states. The measurement of correlation functions of a single photon source that is divided by an appropriate beam splitter is of special interest to the field. However, it is also interesting to analyze the correlation functions of various other types of electromagnetic fields sent through the microwave beam splitter.

In this bachelor thesis, the behavior of beam splitters in a cryogenic setup was determined and the theory of correlation functions was reviewed. LabView data acquisition software was written to allow measurements of statistical correlations of the signals entering the data acquisition system. Auto- and cross correlations of coherent and thermal fields as well as mixtures between them were recorded. Corresponding data was analyzed to determine the amplifier noise temperature inside the cryostat. The attenuation and total amplification inside the cryostate setup could be calculated. The measurements of non-time and time-resolved auto- and cross correlations compared well to theory. To show the effect of a blackbody radiation source attached to the input, a quasi thermal field based on a white noise source over a limited bandwidth was generated.

Although the thermal field measurements did not agree with theory, the properties of the measured signals could be understood. The results given in this thesis may pave the way for future experiments incorporating a temperature-controlled resistance acting as a real blackbody emitter. Making use of superconducting qubits as single photon source, the work presented here should also allow measurements of correlation functions of single photons.

# Contents

# 1 Introduction

In optics, the work with beam splitters and correlations functions almost belongs to daily routine. When working with microwave fields in a electrical circuit, a different approach is required. Instead of single half-silvered mirrors, one must use special transmission line circuits to realize a beam splitter. Instead of using photodetectors, unavailable at microwave frequencies, one amplifies signals to detect them with conventional electrical circuitry. In this thesis, I will make use of the microwave counterparts of optical beam splitters that have been presented previously [1], [2], [3] and describe the theoretical and experimental premises required for recording correlation functions.

### Correlation functions

A correlation function is the measure of how two signals of any kind are correlated with each other. In optics, these functions may be used to show spatial or temporal differences between two light paths or determine coherence properties of a light source. Therefore, correlation functions also determine the *degree of coherence* of a source of photons. One can distinguish between autocorrelations and cross correlations, i.e. the correlation between a signal and itself and the correlation of two different signals.

The use of correlation functions is not restricted to the field of optics. There are also applications for financial mathematics, general signal processing, music recording and statistics and probability theory.

However, a well known application for correlation function measurements can be found in optics: the classical beam splitting experiment [4], [5]. Sending a light beam emitted from a source that creates only one photon (i.e. a single photon source) to a 50:50 beam splitter divides the beam into two light paths, see Fig. 1.1 a). These paths are directed into coincidence counters which can detect the presence of single photons. It is now important to notice that it is not possible to detect one photon at both detectors at the same time, i.e. the single photon created either passes the upper or lower path, but never both simultaneously. One can then record the counting statistics of both detectors (i.e. the photon counts) in dependence on time and calculate the correlation between the two measurements. As the photon counts can never appear simultaneously, the signals are perfectly anticorrelated for zero time-difference.

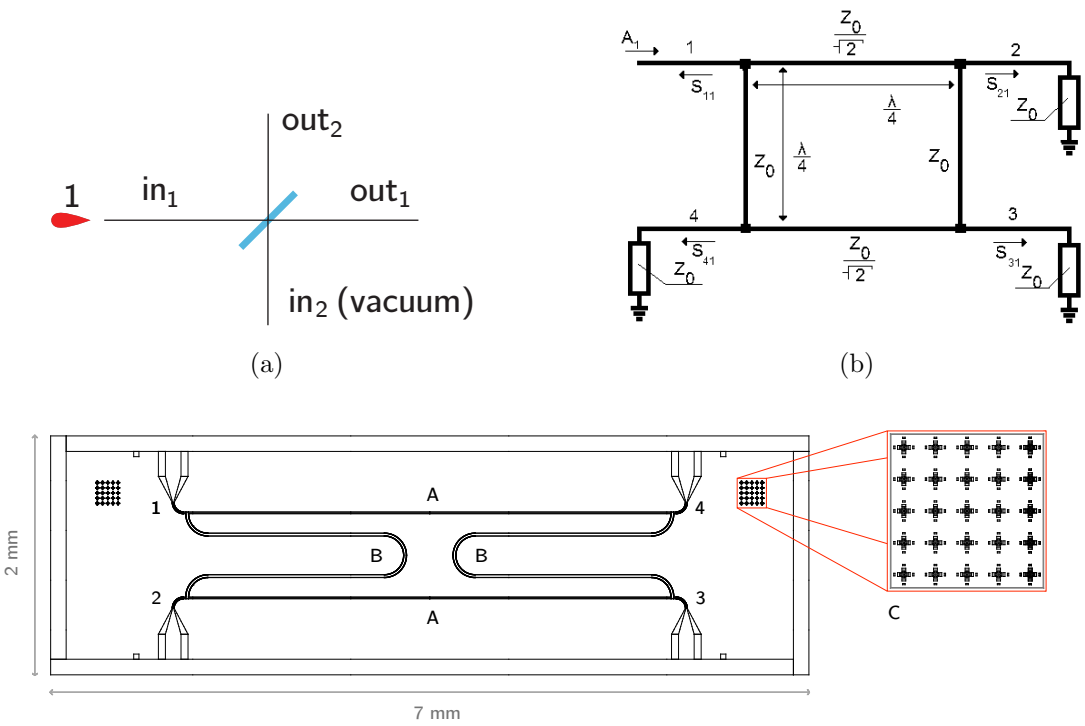


Figure 1.1: a) Sketch of optical beam splitter. b) Schematic of the electrical circuit of a microwave quadrature hybrid. c) Coplanar waveguide design of the quadrature hybrid used in this project. (1) to (4) denote the port number. Niobium CPW lines each have a length of 4670 $\mu$m: lines (A) correspond to an impedance of $Z_0 = 50\,\Omega$ whereas lines (B) correspond to $Z_0/\sqrt{2} = 35.35\,\Omega$. CPW dimension are given by $a_1 = 5.0\,\mu$m and $b_1 = 9.5\,\mu$m for $Z_0 = 50\,\Omega$ and $a_2 = 12.0\,\mu$m and $b_2 = 15.0\,\mu$m for $Z_0/\sqrt{2} = 35.35\,\Omega$. In (C) alignment markers are illustrated. Figures taken from [1].

### Microwave beam splitters

In optics, one can use optical beam splitters and two detectors to measure the correlation functions of the outputs. Working with microwave frequency radiation, one needs to consider new devices working in this frequency range that are also suitable for experiments in circuit quantum electrodynamics. Devices discussed in [1], [2] and [3] provide appropriate characteristics for this field. The microwave beam splitters are fabricated on a superconducting microchip using coplanar waveguide transmission lines, see Fig. 1.1 c). The geometries needed for the device are sketched in Fig. 1.1 b). With niobium as superconducting thin film on a sapphire substrate, the device must be cooled down below its critical temperature of 9.2 K. In previous experiments this was done by using a dipstick plunged into liquid helium. To analyze the properties of the beam splitter, one may make use of a microwave generator. The simplest way is to take a Vector Network Analyzer (VNA) that generates a signal, sends it through the device and measures transmission and reflection of the circuit in a phase sensitive way. The

transmission loss (or scattering matrix parameter) is a logarithmic magnitude that can be used to determine whether the splitting device works adequately. That means that the ingoing signal needs to be split equally to the two outputs, which corresponds to a transmission loss of $-3$ dB each. In addition, the beam splitter should work over a frequency range of 1-2 GHz.

### Measuring correlation functions in the GHz range

With these devices, one can try to measure correlation functions in the GHz range. In order to facilitate single photon measurements, a temperature of 20 mK is required to ensure that typical thermal fluctuations range much below quanta corresponding to single photon transitions [6]. One therefore uses a cryostat to create a superconducting environment instead of dipping the sample into liquid helium inside a dewar. The beam splitter then needs to be connected to microwave electronics via various cables in- and outside the cryostat. A set of amplifiers and attenuators that keep the power of the signal in the right range is needed to record the signals at a data acquisition card afterwards. As amplifiers add thermal noise to the signal, a mixture between a thermal field and the specific field created at the input needs to be considered. By using two independent amplifiers, one can eliminate the noise when recording cross correlations. For a detailed description of the measuring setup, see chapter 3.1.

### Circuit Quantum Electrodynamics

In circuit quantum electrodynamics (circuit QED) the interaction between light and matter is investigated. Superconducting circuits acting as artificial atoms (qubits) can be placed on superconducting microchips and coupled to microwave resonators [7]. Accompanied by fabrication techniques well known from integrated circuit manufacturing, this gives rise to a highly scalable and controllable two-level system that can be read out easily. Recent work has been done on examining sideband transitions between transmission line resonator and qubit [8]. In future, transitions in the circuits could be used as single photon emitters.

# 2 Theory

## 2.1 Correlation functions

One can distinguish between first- and second-order coherence functions. First-order coherence functions relate to correlations of the fields and may be used to determine the degree of coherence or coherence length of light. However, one is unable to obtain any statistical information from first-order coherence functions. With the second-order coherence function, which relates to correlations of intensities rather than fields, this becomes possible. Although this thesis concentrates on second-order coherence functions mainly, in the following section both cases are discussed.

### First-order coherence

For two points in space at time t, $x_1 = (\mathbf{r_1}, t)$ and $x_2 = (\mathbf{r_2}, t)$, the normalized first-order coherence function reads [4]

$$g^{(1)}(x_1, x_2) = \frac{tr\{\hat{\rho}\hat{E}^{(-)}(x_1)\hat{E}^{(+)}(x_2)\}}{\sqrt{tr\{\hat{\rho}\hat{E}^{(-)}(x_1)\hat{E}^{(+)}(x_1)\}\, tr\{\hat{\rho}\hat{E}^{(-)}(x_2)\hat{E}^{(+)}(x_2)\}}} \tag{2.1}$$

$$= \frac{\langle\hat{E}^{(-)}(x_1)\hat{E}^{(+)}(x_2)\rangle}{\sqrt{\langle\hat{E}^{(-)}(x_1)\hat{E}^{(+)}(x_1)\rangle\, \langle\hat{E}^{(-)}(x_2)\hat{E}^{(+)}(x_2)\rangle}}, \tag{2.2}$$

where it has been used that the expectation value of a quantum mechanical observable $\hat{A}$ is given by $\langle\hat{A}\rangle = tr\{\hat{\rho}\hat{A}\}$, with $\hat{\rho}$ the density operator to the corresponding state. $\hat{E}^{(+)}$ is the component of the electromagnetic field that describes absportion (called positive frequency part). In the Heisenberg picture it is given by

$$\hat{E}^{(+)}(\mathbf{r}, t) = i\sum_{\mathbf{k},s}\sqrt{\frac{\hbar\omega_k}{2\epsilon_0 V}}\mathbf{e}_{\mathbf{k}s}\hat{a}_{\mathbf{k}s}(t), \tag{2.3}$$

summing over all modes with wave vector $\mathbf{k}$ and polarisation $s$. This expression also contains the frequency $\omega_k$ corresponding to the wave vector by $\omega_k = c\mathbf{k}$, a volume $V$ in $\mathbf{k}$-space, the polarization vector $\mathbf{e}_{\mathbf{k}s}$ and the field annihilation operator $\hat{a}_{\mathbf{k}s}(t)$. The

negative frequency part corresponding to emission $\hat{E}^{(-)}$ is simply the complex conjugate of $\hat{E}^{(+)}$:

$$\hat{E}^{(-)}(\mathbf{r},t) = \left[\hat{E}^{(+)}(\mathbf{r},t)\right]^{\dagger}. \tag{2.4}$$

The total electromagnetic field consisting of both positive and negative frequency parts is then

$$\hat{E}(\mathbf{r},t) = \hat{E}^{(+)}(\mathbf{r},t) + \hat{E}^{(-)}(\mathbf{r},t). \tag{2.5}$$

Instead of explicitly writing the coherence function in terms of space and time, one can, assuming the case of an one-dimensional transmission line, express spatial differences $x_2 - x_1$ as temporal differences by relating $\tau = (x_2 - x_1)/c$ and hence write

$$g^{(1)}(x_1, x_2) = g^{(1)}(\tau). \tag{2.6}$$

### Second-order coherence

The second-order coherence function (which is also sometimes denoted as degree of second-order coherence) is given by [4], [9]

$$g^{(2)}(\tau) = \frac{\langle \hat{E}^{(-)}(t)E^{(-)}(t+\tau)\hat{E}^{(+)}(t+\tau)\hat{E}^{(+)}(t)\rangle}{\langle \hat{E}^{(-)}(t)\hat{E}^{(+)}(t)\rangle \langle \hat{E}^{(-)}(t+\tau)\hat{E}^{(+)}(t+\tau)\rangle}, \tag{2.7}$$

where $\tau = t_2 - t_1$ is the time difference between two photon counts. For single-mode planar fields, i.e.

$$\hat{E}^{(+)}(t) = i\sqrt{\frac{\hbar\omega_k}{2\epsilon_0 V}}\hat{a}e^{i(\mathbf{kr}-\omega t)} \tag{2.8}$$

one can write Eq. (2.7) in terms of ladder operators and gets [4]:

$$g^{(2)}(\tau) = \frac{\langle \hat{a}^{\dagger}\hat{a}^{\dagger}\hat{a}\hat{a}\rangle}{\langle \hat{a}^{\dagger}\hat{a}\rangle^2} = \frac{\langle n(n-1)\rangle}{\langle n\rangle^2} \tag{2.9}$$

$$= 1 + \frac{\langle (\Delta n)^2\rangle - \langle n\rangle}{\langle n\rangle^2}, \tag{2.10}$$

with $\langle n\rangle$ the average number of photons and $\langle (\Delta n)^2\rangle$ the variance.

As statistical properties vary from field to field, one needs to distinguish between the appropriate correlation function according for each of those.

### 2.1.1 Second order correlation function for coherent fields

Considering a coherent field, one can see by writing the coherent states $|\alpha\rangle$ in a fock-state basis [10]

$$|\alpha\rangle = e^{-\frac{|\alpha|^2}{2}} \sum_{n=0}^{\infty} \frac{\alpha^n}{\sqrt{n!}} |n\rangle = e^{-\frac{|\alpha|^2}{2}} e^{\alpha \hat{a}^\dagger} |0\rangle , \tag{2.11}$$

that these types of fields have Poissonian photon number statistics

$$P(n) = e^{-\langle n \rangle} \frac{\langle n \rangle^n}{n!}. \tag{2.12}$$

For Poissionian statistics the variance equals the mean, i.e in terms of mean photon numbers

$$\langle n \rangle = \langle (\Delta n)^2 \rangle \tag{2.13}$$

by combining equations (2.10) and (2.13) one obtains following important expression for coherent fields:

$$g^{(2)}(0) = g^{(2)}(\tau) = 1. \tag{2.14}$$

This is an important result, as this expression is not time dependent.

### 2.1.2 Correlation function for thermal fields

For thermal fields, i.e. black body radiation, the mean photon number (Bose-Einstein-Distribution) is given by:

$$\langle n_T \rangle = \frac{1}{e^{\hbar\omega/kT} - 1}, \tag{2.15}$$

with $k$ the Boltzmann constant, $T$ temperature, $\hbar$ the reduced Planck's constant and $\omega$ the frequency. The correlation function of a thermal field is then determined by

$$g^{(2)}(\tau) = 1 + \left| g^{(1)}(\tau) \right|^2 . \tag{2.16}$$

It can be found in [11], [12], that the expression of temporal coherence is given by

$$\gamma(0, \tau) = \frac{90}{\pi^4} \zeta(4, 1 + kT/\hbar\, i\tau), \tag{2.17}$$

where $\zeta$ is the Riemann zeta function normalized by the prefactor $90/\pi^4$ to 1. By definition of $\gamma$ [11]

$$\gamma(x_1, x_2) = \frac{\langle \hat{E}^{(-)}(x_1) \hat{E}^{(+)}(x_2) \rangle}{\sqrt{\langle \hat{E}^{(-)}(x_1) \hat{E}^{(+)}(x_1) \rangle \langle \hat{E}^{(-)}(x_2) \hat{E}^{(+)}(x_2) \rangle}}, \tag{2.18}$$

one can immediately see that temporal coherence is exactly the same as first-order coherence introduced in Eq. (2.2),

$$\gamma(x_1, x_2) = g^{(1)}(x_1, x_2), \tag{2.19}$$

and with Eq. (2.16) and (2.17) it follows:

$$g^{(2)}(\tau) = 1 + \left| \frac{90}{\pi^4} \zeta(4, 1 + kT/\hbar\, i\tau) \right|^2 . \tag{2.20}$$

### 2.1.3 Mixtures of thermal and coherent fields

For mixtures of thermal and coherent radiation important statistical properties of the field can be found [13], [14]. The total mean photon number $\langle n \rangle$ is given by

$$\langle n \rangle = \langle n_C \rangle + \langle n_T \rangle \,, \tag{2.21}$$

i.e. the sum of the mean contributions of coherent $\langle n_C \rangle$ and thermal radiation $\langle n_T \rangle$. Further, one can find the variance of the total photon number equals

$$\langle (\Delta n)^2 \rangle = 2 \langle n_C \rangle \langle n_T \rangle + \langle n_C \rangle + \langle n_T \rangle^2 + \langle n_T \rangle \,. \tag{2.22}$$

By substituting in Eq. (2.21) and (2.22) into Eq. (2.10)

$$g^{(2)}(0) = 1 + \frac{\langle (\Delta n)^2 \rangle - \langle n \rangle}{\langle n \rangle^2} \tag{2.23}$$

$$= 1 + \frac{2 \langle n_C \rangle \langle n_T \rangle + \langle n_C \rangle + \langle n_T \rangle^2 + \langle n_T \rangle - (\langle n_C \rangle + \langle n_T \rangle)}{(\langle n_C \rangle + \langle n_T \rangle)^2}, \tag{2.24}$$

one finally obtains following expression for the correlation function:

$$g^{(2)}(0) = 1 + \frac{2 \langle n_C \rangle \langle n_T \rangle + \langle n_T \rangle^2}{(\langle n_C \rangle + \langle n_T \rangle)^2}. \tag{2.25}$$

### 2.1.4 Cross- and Autocorrelation function

Proceeding from quantum mechanical definitions of coherence functions one arrives at the expressions for auto- and cross correlations. The cross correlation function describes the correlation between two signals $A_1^2$ and $A_2^2$ given by

$$g^{(2)}(\tau) = \frac{\langle A_1^2(t) A_2^2(t+\tau) \rangle}{\langle A_1^2(t) \rangle \langle A_2^2(t) \rangle}, \tag{2.26}$$

where $A_i^2$ are the squared amplitudes. To measure the correlation of one signal (i.e. one output line) with itself, one can write the autocorrelation function as

$$g^{(2)}(\tau) = \frac{\langle A_{1,2}^2(t) A_{1,2}^2(t+\tau)\rangle}{\langle A_{1,2}^2(t)\rangle^2}, \tag{2.27}$$

which has been obtained directly from Eq. (2.26).

# 3 Correlation Function Measurements

## 3.1 Experimental Setup

Previous work [2], [1] has been done on analyzing the behavior of beam splitter devices at the temperature of 4.2 K. This was realized by using a dipstick that was clamped at the neck of dewar filled with liquid helium. By releasing an O-ring clamp, the dipstick could be lowered and the device cooled without much effort. However, this temperature is too high to perform measurements introduced in chapter 2. Temperatures in the range of 4.2 K add too much thermal radiation to successfully perform autocorrelation or cross correlation measurements. Amplifier thermal noise contributions (see chapter 3.2.2) in the same temperature ranges could not be distinguished from the background fields. In addition, for incorporating superconducting qubits as single photon source, one needs to ensure that thermal fluctuations $kT$ range below the energies corresponding to qubit transition frequencies $\omega \approx 6$ GHz, i.e. $kT \ll \hbar\omega$ [6]. This can be achieved by using a dilution refrigerator (*VeriCold*), in which temperatures can reach below 15 mK. A dilution fridge is cooled by diluting helium isotopes $^3$He and $^4$He and dissipating energy from the system [15]. The cryogenic wiring is schematically depicted in Fig. 3.1.

Microwave signals that are sent into the refrigerator are created at room temperature with a microwave generator and connected via semi rigid coaxial cables to the top input of the cryostat. After being attenuated at different temperature stages of the cryostat, the signal interacts with the on-chip beam splitter fixed in a sample mount at cryogenic temperatures of $\approx 15$ mK and is split into two outgoing signals of about equal amplitude. The output microwave then passes through two circulators, to prevent thermal noise from the subsequent low-temperature amplifier from traveling back to the sample. After a second warm amplification the RF signal is mixed with a local oscillator (LO) and is downconverted to an IF frequency of 10 MHz. To ensure a well defined phase difference between both outputs and the LO and avoid the necessity of operating a second LO, the LO was divided into two signals with a splitter and then linked to both IQ-mixers. Due to the additional splitter, the LO needs to be operated at 4 dB higher power, i.e. in our measurements at 16 dBm. A third amplification at the IF follows and after a low-pass filter with bandwidth of 35 MHz the signal is digitally recorded on a PC using a data acquisition card. LabView program *CleanSweep* enables to analyze measured data and remotely control all room-temperature microwave electronics. For

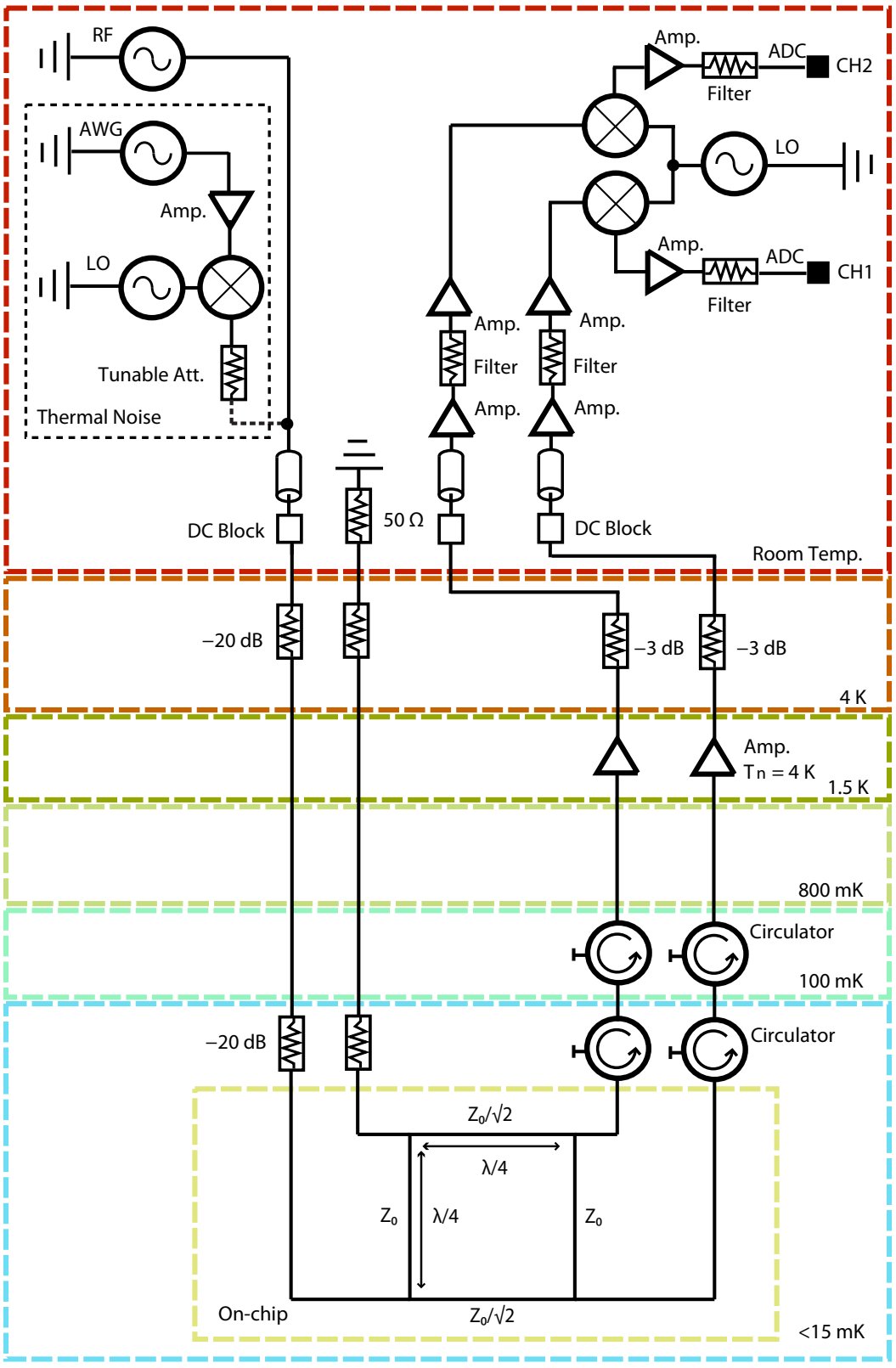


Figure 3.1: Sketch of VeriCold cryostat experimental setup. See text for detailed description.

a detailed discussion of the cryogenic measurement setup, see also [16].

### 3.1.1 Implementation of Correlation function routines in LabView

In order to carry out simultaneous cross- and autocorrelation measurements, CleanSweep had to be adapted slightly. After the LabView program was made capable of recording both channels, I created a sub-VI that handles measured data. For $\tau = 0$ the sub-VI calculates the mean of an incoming signal:

$$\langle A_{1,2}^2 \rangle = \frac{1}{N} \sum_{t=1}^{N} A_{1,2}^2(t), \tag{3.1}$$

with $A_i^2$ the measured squared amplitude in Volts and $N$ the number of data points acquired. The autocorrelation is given by

$$g^{(2)}(0) = \frac{\frac{1}{N}\sum_{t=1}^{N} A_1^4(t)}{\left(\frac{1}{N}\sum_{t=1}^{N} A_1^2(t)\right)^2}, \tag{3.2}$$

with $A_i$ and N as above. The cross correlation then reads:

$$g^{(2)}(0) = \frac{\frac{1}{N}\sum_{t=1}^{N} A_1^2(t)A_2^2(t)}{\frac{1}{N}\sum_{t=1}^{N} A_1^2(t)\frac{1}{N}\sum_{t=1}^{N} A_2^2(t)}. \tag{3.3}$$

In the time dependent case, i.e. for time-resolved correlation functions, I took prebuilt LabView sub-VIs called *AutoCorrelations* and *CrossCorrelations*. The sub-VI's algorithms correspond to following equations:

$$g^{(2)}(\tau) = \frac{\frac{1}{N-|\tau|}\sum_{t=1}^{N} A_1^2(t)A_1^2(t+\tau)}{\left(\frac{1}{N}\sum_{t=1}^{N} A_1^2(t)\right)^2} \tag{3.4}$$

for the time-resolved autocorrelation. Factor $1/(N-|\tau|)$ corresponds to a normalization correction for the offsets. In software, this can be taken into account by choosing setting *unbiased* in the sub-VI. One must consider that the difference $N - |\tau|$ makes sense as $N$ is the number of data points acquired in a certain time. By knowing the time separation between each data point, one can express the time difference $\tau$ as an offset corresponding to a certain number of measuring points.

The time-resolved cross correlation yields:

$$g^{(2)}(\tau) = \frac{\frac{1}{N-|\tau|}\sum_{t=1}^{N} A_1^2(t)A_2^2(t+\tau)}{\frac{1}{N}\sum_{t=1}^{N} A_1^2(t)\frac{1}{N}\sum_{t=1}^{N} A_2^2(t)} \tag{3.5}$$

In both equations above the enumerator is calculated by the corresponding sub-VIs introduced in the last paragraph.

As one can see directly, these expressions match the definitions given in chapter 2.

## 3.2 Non-time resolved experiments

The first experiments that were done with the VeriCold setup described in section 3.1 were non-time resolved. The behavior of the beam splitter under cryogenic conditions had to be analyzed and compared with previous dipstick measurements.

### 3.2.1 Beam splitter measurements at 20 mK

After the beam splitter device (sample Z2) had been cooled down to 20 mK, the fridge was connected to the measurement setup according to Fig. 3.1 so that both beam splitter output lines could be read out separately and, for later measurements, also simultaneously. All measurements were performed with the LabView data acquisition program *CleanSweep*, that allowed to control microwave generators (i.e RF, LO), signal generators (AWG) and trigger sources remotely. In Fig. 3.2 a) a beam splitter analysis at cryogenic temperatures is depicted and compared with a previous dipstick measurement (Fig. 3.2 b)). The VeriCold measurement was performed sweeping the frequency in a range from 3 to 9 GHz.

To compare VeriCold to dipstick measurements, amplitudes of the cryostat measurements were normalized to 0.5 with respect to the working frequency of 6.5 GHz. It can be seen in Fig. 3.2 b) that in the dipstick measurement the signals do not match perfectly at half power, corresponding to a slight asymmetric splitting. These results have already been seen before and were discussed in [1], [2]. In the VeriCold setup, see Fig. 3.2 a), the deviation seems to be reduced. However, it is highly likely that this is by virtue of unequal amplification of the output channels. Subsequent oscillatory features in Fig. 3.2 a) are due to the strong frequency dependence of the warm amplifier chain (i.e. downconversion board).

### 3.2.2 Auto- and cross correlations and mean amplitude squared

The measurements described in the previous section have shown it can be assumed that the beam splitter works reliable enough in the cryogenic setup to continuing further experiments. Therefore, an experiment recording the Auto- and cross correlations (see chapter 2) of beam splitter output channels could was set up. The amplitude of the

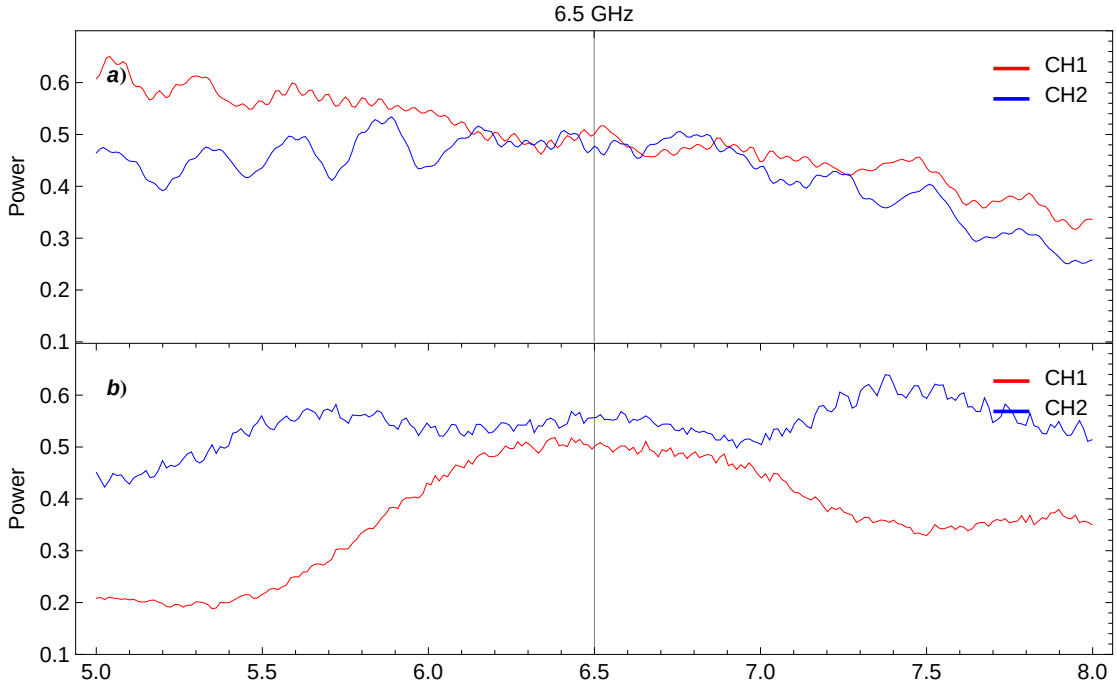


Figure 3.2: Comparison of beam splitter measurement inside a) the cryostat at 20 mK and b) inside the dipstick at 4.2 K.

signal going into the data acquisition card on the measuring PC was squared and second order auto- and cross correlations were calculated according to Eq. (2.26) and (2.27).

The Auto- and cross correlation measurements, see Fig. 3.3 were recorded with a coherent RF input at a fixed frequency of 6.5 GHz (i.e. the working frequency of the beam splitter) and swept over different RF input powers. The LO was set to 6.51 GHz, corresponding to a heterodyne intermediate frequency (IF) of 10 MHz. By virtue of the measurement setup, one has to bear in mind that cold amplifiers at a temperature stage of 1.4 K give rise to noise and produce a quasi thermal field characterized by a certain noise temperature. Therefore, one has to consider that the actual output corresponds to a mixture between a thermal and a coherent field (also see chapter 2.1.3), rather than to just the coherent field alone. Hence, the output power (or amplitude squared) in dependence on the input RF power was recorded as this illustrates the mixture of thermal and coherent fields at different powers nicely.

### Autocorrelation

The autocorrelation function of the two output channels (i.e. two split output lines) is displayed in Fig. 3.3 b). At low powers of the coherent tone, thermal field contributions are much larger than the ones of the coherent field. Thus, coherent fields can be

neglected:

$$g^{(2)}(0) \xrightarrow{\langle n_C \rangle \to 0} 2, \tag{3.6}$$

which relates excactly to the measurement. For increasing powers, a coherent contribution can be detected and

$$g^{(2)}(0) \xrightarrow{\langle n_C \rangle \to \infty} 1, \tag{3.7}$$

which is also true for this measurement. For power ranges in between these limits, one can apply Eq. (2.25) directly. As the mean number of coherent photons $\langle n_C \rangle$ is proportional to the input power $P$ and the mean number of thermal photons $\langle n_T \rangle$ is proportional to the Bose-Einstein distribution (c.f. Eq. (2.15)) one can fit the data with

$$g^{(2)}(0) = 1 + \frac{2A^2\beta + \beta^2}{(\beta + A^2)^2}, \tag{3.8}$$

which can directly be obtained from Eq. (2.25). $A^2$ and $\beta$ (both in units of $V^2$) are including the fit parameters $\gamma$ and $T$ (fitted temperature) and are given by:

$$\beta = \frac{F_{\text{amp}}\, R\, \hbar\omega\, d\nu}{e^{\hbar\omega/kT} - 1}, \tag{3.9}$$

$$A^2 = \gamma\, P\, R \tag{3.10}$$

with $k$ the Boltzmann constant, $\hbar$ the reduced Planck's constant, $\omega = 2\pi\nu$ the frequency, $d\nu = 35$ MHz the bandwidth, $R = 50\,\Omega$ the resistance and $P$ the input power in W. The conversion between input power in W and voltage squared (i.e. amplitude squared) is simply given by:

$$P = \frac{V^2}{R}. \tag{3.11}$$

The factor $F_{\text{amp}} = 107.8 \pm 1.5\,\text{dB} \approx 6 \pm 2 \cdot 10^{10}$ is needed to take the amplification inside the VeriCold setup into account and was estimated from previous calibration measurements. Based on the estimated amplification factor $F_{\text{amp}}$, fitting the function gives rise to a temperature of $T = 5.3 \pm 2.2$ K[1] and a factor $\gamma = 5700 = 38$ dB. $\gamma$ describes the total amplification and attenuation happening inside the measurement setup, therefore already including the factor $F_{\text{amp}}$ defined before:

$$\gamma = F_{\text{amp}} \cdot F_{\text{att}}. \tag{3.12}$$

With a fixed $F_{\text{amp}}$ one can then easily calculate the attenuation $F_{\text{att}} = \gamma / F_{\text{amp}} \approx -70$ dB, which agrees with estimates based on warm calibrations of the cabling setup.

[1] All fit parameters given in this context illustrate the mean of two fits that have been carried out on both channels depicted in Fig. 3.3 seperately.

### Mean amplitude squared

As mentioned before, one can also acquire the mean squared amplitudes (in units of $V^2$) of both channels, see Fig. 3.3 a). As the output power should be proportional to the input, one can easily fit following line to the measurement:

$$\langle A^2 \rangle = \beta + A^2, \tag{3.13}$$

with $\beta$ and $A^2$ as above. Assuming an amplification factor of $F_{\text{amp}} = 107.8 \pm 1.5$ dB as before, one gets a fitted temperature of $T = 6.0 \pm 2.4$ K.

Both experiments showed amplification noise temperatures that agree quite well with datasheet values of $T \approx 4$ K. However, one has to be aware of an uncertainty in the cold amplification of the setup, as it could only be calibrated at room temperature leading to differences in the behavior of cold amplifiers as well as attenuation of microwave coaxial cables.

### Cross correlation

Measuring cross correlations, one does not have to consider a mixture of thermal and coherent field any more. Since the two output channels are amplified with independent amplifiers, their noise is uncorrelated, and can be averaged out. Neglecting thermal contributions, one can assume a fully coherent field with a constant cross correlation value $g^{(2)}(\tau) = 1$. This is consistent with our measurements, see Fig. 3.3 c).

In fact there is a little thermal contribution due to the radiation background in the sample mount corresponding to temperatures of $\approx 20$ mK. However, features according to this temperature could not be resolved. Fig. 3.4 illustrates a theoretical cross correlation function with thermal contributions of different temperatures. For a thermal field with temperature of 4 K (i.e. like in the previous autocorrelation function measurements for the amplifier noise), a curve can be measured easily. At lower temperatures, i.e. 0.02 K = 20 mK corresponding to the thermal background, the slope of the theoretical curve at zero power is too narrow to be detected.

## 3.3 Time resolved experiments

The next important step was to record both time dependent Auto- and cross correlations as already introduced in chapter 2. To record corresponding data, one could use the same setup as in the non time-depedent case but had to modify LabView program CleanSweep slightly. This was accomplished by creating an additional sub-VI according to the equations presented in section 3.1.1.

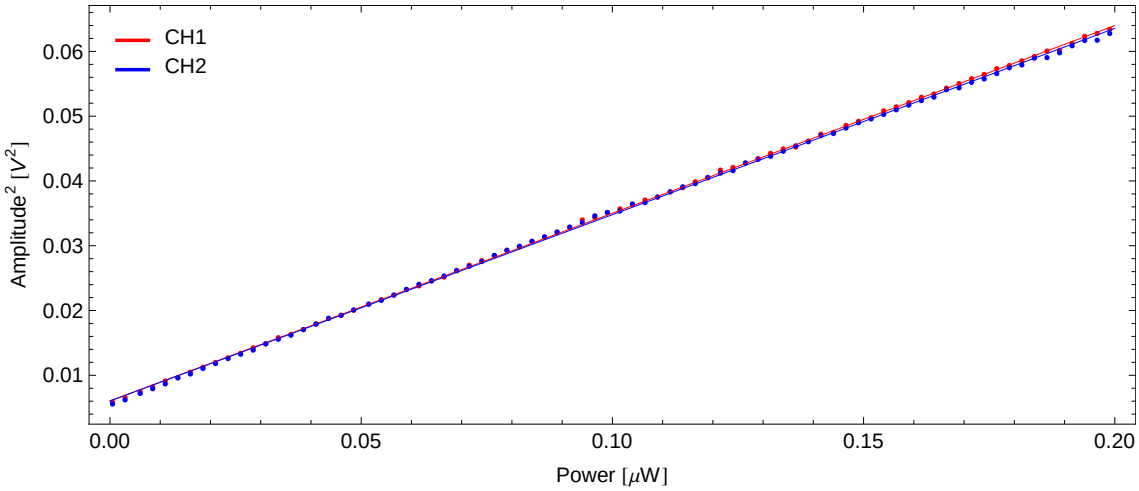


(a)

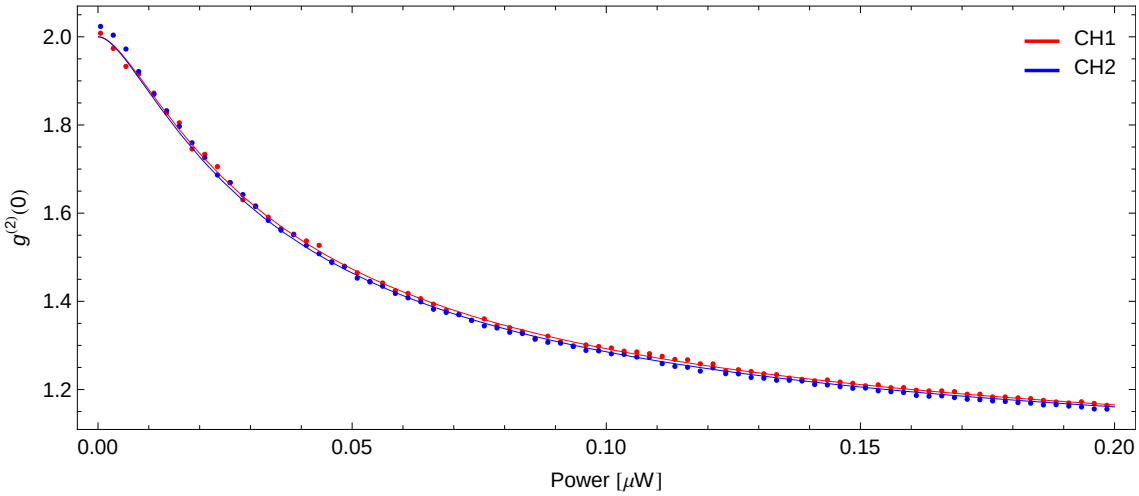


(b)

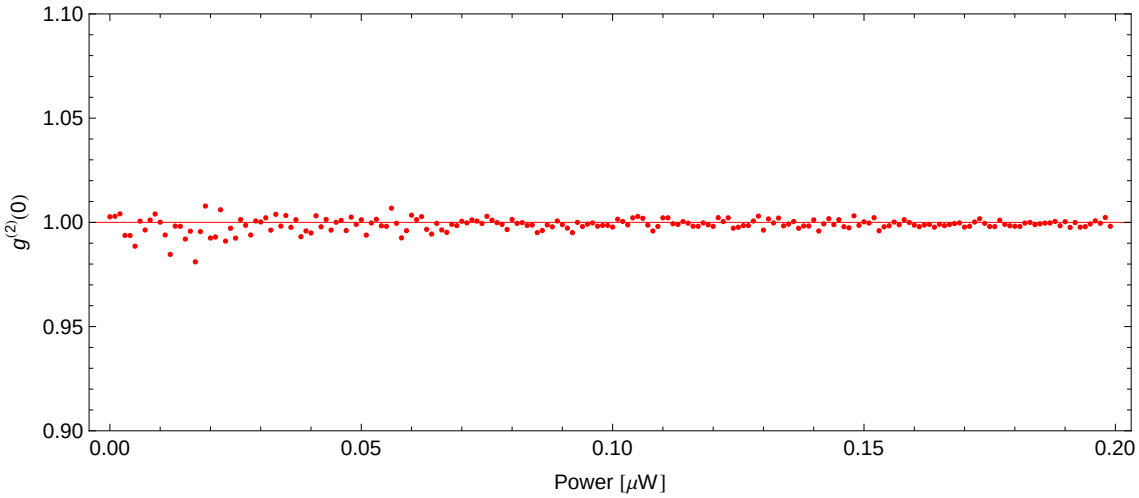


(c)

Figure 3.3: Measured a) mean square amplitude and b) $\tau = 0$ autocorrelation and c) cross correlation function of channels 1 and 2 inside the VeriCold. Recorded data is plotted as points, a theory fit is displayed by solid lines.

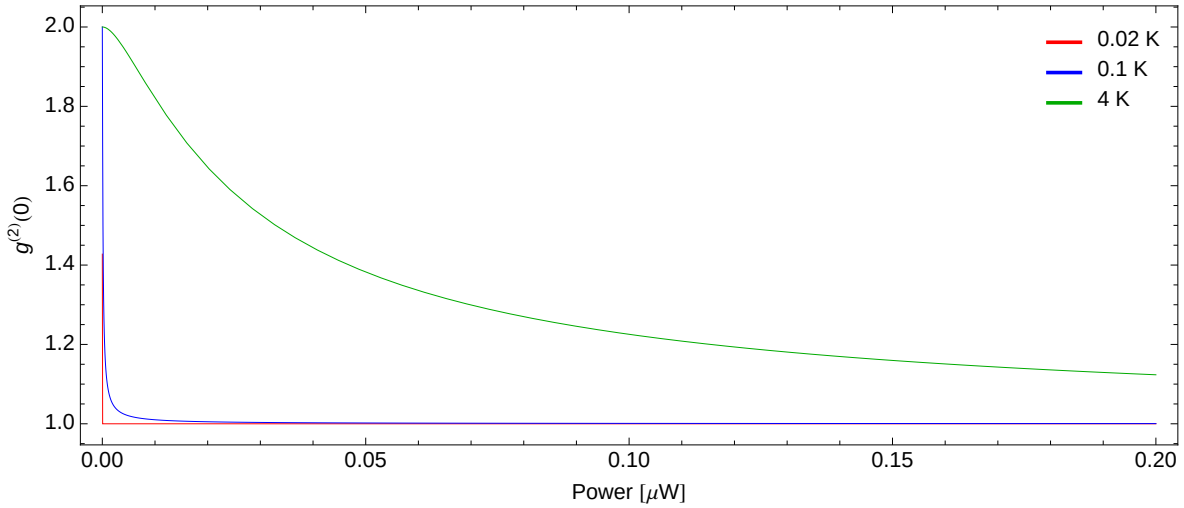


Figure 3.4: Plot shows the theoretical behavior of a simulated cross correlation function with respect to an additional thermal field at different temperatures. The curve for T = 0.02 K, corresponding to background thermal radiation in the cryostat, could not be resolved in our measurements.

### Time resolved Autocorrelation

In the case of the autocorrelation function one has once again to consider a mixture of a coherent and a thermal field caused by the amplifiers. Figures 3.5 a) and b) display measurement data and the theoretical curve. Theory predicts the autocorrelation function of mixtures of thermal and coherent fields to behave like Eq. (2.20), i.e. a Riemann zeta function. This function has a strong dependence on temperature $T$ and gets very narrow for temperatures of about 6 K (i.e. a corresponding full width at half maximum of $10^{-12}$ s). Therefore, it was impossible to resolve this feature within the limits of our experimental setup. Therefore, in Fig. 3.5 b) a theoretical plot of the function proposed before rather than a real data fit is shown. For smaller temperatures, i.e. in the range of 0.1 K, the full width at half maximum of the Riemann zeta function increases to $10^{-10}$ s, which is also too narrow to resolve in our current setup. In Fig. 3.5 b), notice that as the range had to be cut off to display the function, only one data point is left at $\tau = 0$.

### Time resolved cross correlation functions

As seen before, when measuring the cross correlation of the two output ports of the beam splitter, the thermal field created at the amplifier cancels out. Therefore one expects the same behavior as for the non time-resolved case, i.e. a constant value of 1. This is exactly what can be seen in Fig. 3.5 c). The small thermal background field that should exist would be difficult to resolve because of the considerations discussed in the previous section.

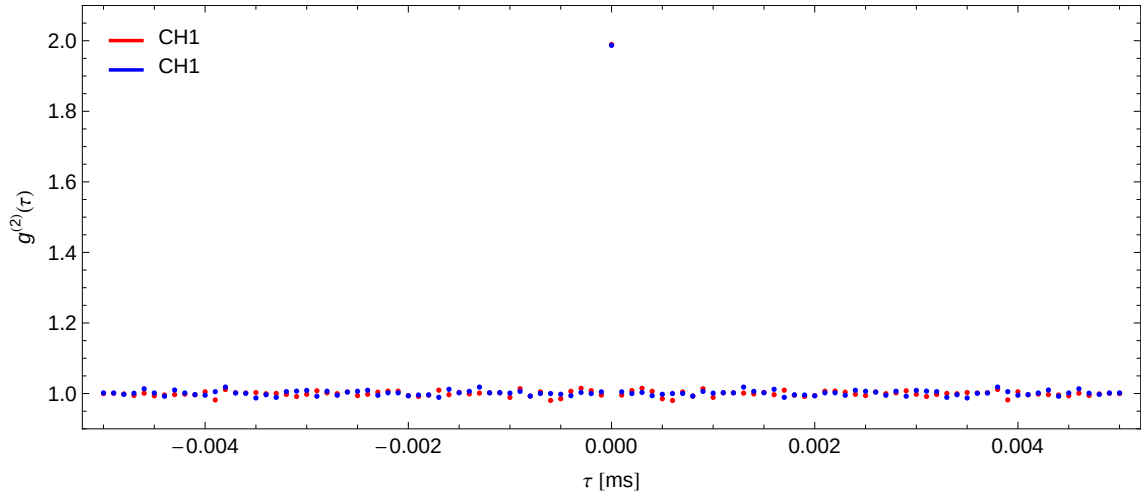


(a)

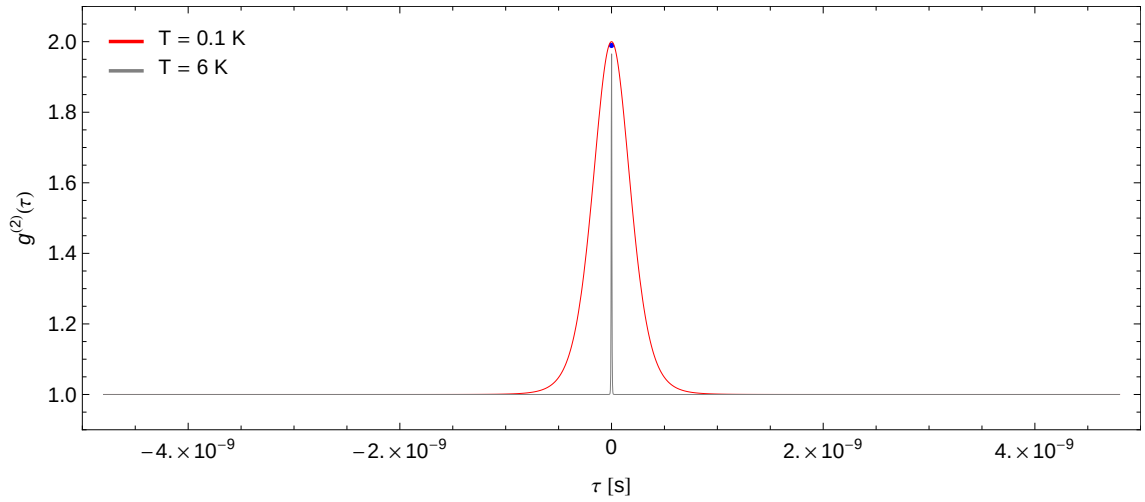


(b)

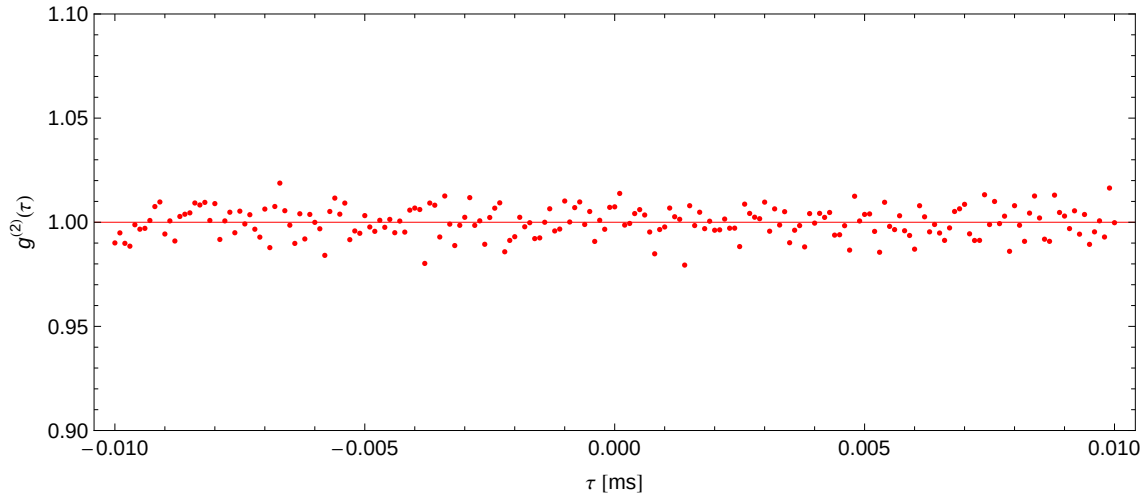


(c)

Figure 3.5: a) and b) Measurements of time dependent autocorrelation function for mixtures of thermal and coherent field at channels 1 and 2. In b) the theory autocorrelation function is plotted for different temperatures. c) Measured time dependent cross correlation (points) and a theoretical fit (solid line).

## 3.4 Generation of artifical thermal noise

After measuring basic time-dependent and time-independent correlations functions of the microwave beam splitter one could proceed to approach more advanced experiments. To see how different types of input fields affect the correlation functions, we planned to apply a thermal field to one of the input ports of the beam splitter inside the cryostat. As this basically requires some changes to the experimental setup we decided to create artificial quasi thermal radiation based on a white noise signal with a bandwith of 500 MHz centered around the operation frequency of 6.5 GHz. This technique has been used previously [17], [18] to perform circuit QED experiments at elevated temperatures. In Fig. 3.1 the thermal noise setup is sketched. Before mixing the signal with an local oscillator (LO) running at 6.5 GHz with 20 dBm, the white noise is amplified by 25 dB. To control the power of the white noise signal going into the setup, i.e. to vary the effective temperature of the artificial thermal soure, a tunable attenuator is used. The subsequent parts of the setup are the same as used in the previous experiments. The main RF source of the experiment was turned off for thermal noise runs.

### 3.4.1 Cross correlation function for thermal inputs

Again, the added uncorrelated noise of the microwave amplifiers inside the cryostat cancels out when measuring the cross correlation functions. Therefore the measurement should directly show changes in the type of field applied to the input port. Fig. 3.6 shows the main result of this experiment. In this measurement the attenuation was swept from 30 to 0 dB with a step of 1 dB. The conversion between input power (i.e. attenuation) and artificial blackbody temperature can be done by using the Bose-Einstein factor (Eq. (2.15)) and a calibration carried out in [18]. In this work it was found that one photon in the cryostat relates to an attenuation of $\approx 33$ dB. However, not truely the same experiment as in [18] was performed. This value might deviate to some amount, as it refers to one photon inside the resonator cavity rather than the beam splitter.

Manipulating Eq. (2.15) one can write the noise temperature $T_{\text{noise}}$ as a function of the mean photon number $\langle n_T \rangle$:

$$T_{\text{noise}}(P) = \frac{\hbar\omega}{k} \frac{1}{\log\left(\frac{1}{\langle n_T \rangle} + 1\right)}. \tag{3.14}$$

As for $\langle n_T \rangle = 1$ the attenuation is $\approx 33$ dB, it follows

$$\langle n_T \rangle (P) = \frac{10^{\frac{33}{10}}}{10^{\frac{P}{10}}} = 10^{(33-P)/10}, \tag{3.15}$$

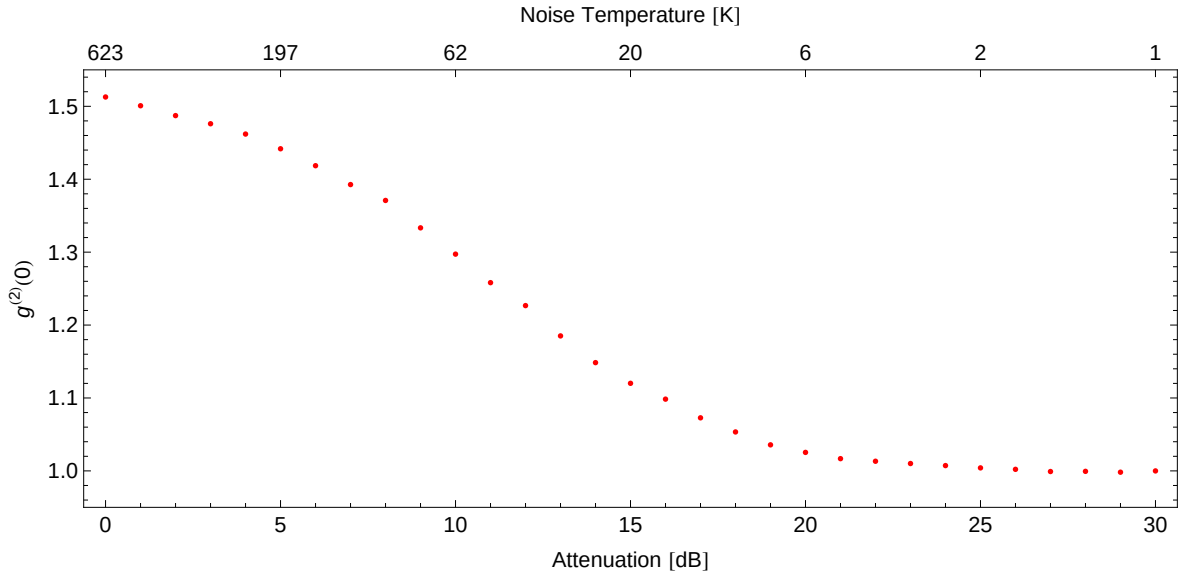


Figure 3.6: Plot illustrates measured cross correlation function with applied artificial thermal field. Attenuation and corresponding temperature are plotted versus the correlation function.

where the conversion $10^{\frac{P}{10}}$ is needed to express the logarithmic dB in a linear scaling. Hence,

$$T_{\text{noise}}(P) = \frac{\hbar\omega}{k} \frac{1}{\log\left(\frac{1}{10^{(33-P)/10}} + 1\right)}. \tag{3.16}$$

Recording the correlation function at $\tau = 0$, the measurement should yield (see Eq. (2.20)):

$$g^{(2)}(0) = 1 + \left|\frac{90}{\pi^4}\zeta(4,1)\right|^2 = 2. \tag{3.17}$$

However, as Fig. 3.6 shows, this is not true. Rather than being flat at $g^{(2)}(0) = 2$ and therefore a real thermal field, the correlation function decreases from 1.5 to 1 in a similiar manner as seen before in the discussion of the autocorrelation function of a mixture between a thermal and coherent field (Fig. 3.3 b)). The coherent field contribution could arise from a leakage when mixing AWG with LO leading to a coherent peak a the LO carrier frequency. Unfortunately it was not possible to fit a function like introduced in Eq. (3.8) to the recorded data with sensible physical constraints. Also, for zero attenuation (i.e. a thermal field with temperature of 623 K), the correlation function stays at 1.5, which does not correspond to theory either. It is likely that the cause of this issue originates from timing deviations of the recorded channels. In theory the correlation function of thermal fields drops rapidly from 2 to 1 (see Fig. 3.5 b)). A very short time delay on one of both channels that could arise even from different cable lengths and therefore already lead to values deviating from theory.

Moreover, it is not certain whether creating blackbody radiation artificially gives rise to the same properties as a real blackbody emitter, i.e. a resistance at a fixed temperature.

In future experiments the reliability of the generated thermal field needs to be checked and compared to other possibilities for its generation.

# 4 Conclusion and Outlook

In this thesis the correlation functions of the two output signals of a microwave beam splitter have been measured. The experiments were done with superconducting devices inside a dilution refrigerator (VeriCold) at 20 mK. Both Auto- and cross correlation have been determined for different types of input fields. Measurements with coherent input fields or mixtures between coherent and thermal fields agreed with theory. An amplifier noise temperature of about 5 K was found, which is close to the specifications. Within the time resolved autocorrelation measurements, the detection resolution was limited and therefore not all theoretical characteristics could be tested. An artificial quasi thermal field based on white noise was generated with an arbitrary waveform generator. The measured cross correlations do not correspond to theory adequately.

In future experiments one needs to verify whether the generation of quasi thermal radiation with an AWG suffices to simulate a blackbody emitter. Temperature controlled resistances could instead be applied inside the cryostat to generate real black body radiation. Incorporating single photon sources, e.g. by using sideband transitions in qubits coupled to a resonator, one could also record the correlation functions and antibunching of a single microwave photon source in the microwave domain.

# Acknowledgements

I want to thank Andreas Wallraff for providing me the possibility to perform my Bachelor thesis at his group. I also want to thank Peter Leek for his support during almost one year of work including my semester thesis. Moreover, I want to acknowledge the help of many group members: Matthias Baur for LabView concerns, Lars Steffen and Romeo Bianchetti for IT support, Johannes Fink for his help with creating thermal noise.

# Bibliography


[1] Littich, G. Superconducting Mach-Zehnder Interferometers for Circuit Quantum Electrodynamics (2009). Semester Thesis.

[2] Henzen, D. Measurement and analysis of superconducting beam splitters (2008). Semester Thesis.

[3] Frey, T. Design of microwave beam splitters (2008). Semester thesis.

[4] Gerry, C. & Knight, P. *Introductory Quantum Optics* (Cambridge University Press, Cambridge, 2005).

[5] Grangier, P., Roger, G. & Aspect, A. Experimental evidence for a photon anti-correlation effect on a beam splitter: A new light on single-photon interferences. *EPL (Europhysics Letters)* **1**, 173–179 (1986). URL `http://stacks.iop.org/0295-5075/1/173`.

[6] Devoret, M. H., Wallraff, A. & Martinis, J. M. Superconducting qubits: A short review. *cond-mat/0411174* (2004). URL `http://arxiv.org/abs/cond-mat/0411174v1`.

[7] Wallraff, A. *et al.* Strong coupling of a single photon to a superconducting qubit using circuit quantum electrodynamics. *Nature* **431**, 162–167 (2004). URL `http://arxiv.org/pdf/cond-mat/0407325`.

[8] Leek, P. J. *et al.* Using sideband transitions for two-qubit operations in superconducting circuits. *Physical Review B* **79**, 180511 (2009). URL `doi:10.1103/PhysRevB.79.180511`.

[9] Walls, D. & Milburn, G. *Quantum optics* (Spinger-Verlag, Berlin, 1994).

[10] Schwabl, F. *Quantenmechanik* (Springer, 2002).

[11] Mehta, C. L. & Wolf, E. Coherence properties of blackbody radiation. i. correlation tensors of the classical field. *Phys. Rev.* **134**, A1143–A1149 (1964).

[12] Kano, Y. & Wolf, E. Temporal coherence of black body radiation. *Proceedings of the Physical Society* **80**, 1273–1276 (1962). URL `http://stacks.iop.org/0370-1328/80/1273`.

[13] Lachs, G. Theoretical aspects of mixtures of thermal and coherent radiation. *Phys. Rev.* **138**, B1012–B1016 (1965).

[14] Lachs, G. Quantum statistics of multiple-mode, superposed coherent and chaotic radiation. *Journal of Applied Physics* **38**, 3439–3448 (1967). URL `http://link.aip.org/link/?JAP/38/3439/1`.

[15] Pobell, F. *Matter and Methods at Low Temperatures* (Springer, 3rd edition,, 2006).

[16] Fink, J. *Single Qubit Control and Observation of Berry's Phase in a Superconducting Quantum Circuit*. Master's thesis, Universität Wien (2007).

[17] Studer, P. Vacuum Rabi Splitting at High Drive Powers and Elevated Temperatures (2008). Diploma Thesis.

[18] Michels, S. Quantum-to-Classical Transition in Circuit Quantum Electrodynamics (2008). Semester Thesis.